HHS Public Access

Author manuscript

Magn Reson Imaging. Author manuscript; available in PMC 2017 May 01.

Published in final edited form as:

Magn Reson Imaging. 2016 May ; 34(4): 535–540. doi:10.1016/j.mri.2015.12.023.

Metabolite-Selective Hyperpolarized ^{13}C Imaging using Extended Chemical Shift Displacement at 9.4T

Seungwook Yang[1], **Joonsung Lee**[2], **Eunhae Joe**[1], **Hansol Lee**[1], **Young-Suk Choi**[3], **Jae Mo Park**[4], **Daniel Spielman**[4], **Ho-Taek Song**[3], and **Dong-Hyun Kim**[1]

[1]Department of Electrical and Electronic Engineering, Yonsei University, Seoul, Korea

[2]Center for Neuroscience Imaging Research, Institute for Basic Science, Sungkyunkwan University, Suwon, Korea

[3]Department of Radiology, College of Medicine, Yonsei University, Seoul, Korea

[4]Department of Radiology, Lucas MRI Center, Stanford University, California, USA

Abstract

Purpose—To develop a technique for frequency-selective hyperpolarized ^{13}C metabolic imaging in ultra-high field strength which exploits the broad spatial chemical shift displacement in providing spectral and spatial selectivity.

Methods—The spatial chemical shift displacement caused by the slice-selection gradient was utilized in acquiring metabolite-selective images. Interleaved images of different metabolites were acquired by reversing the polarity of the slice-selection gradient at every repetition time, while using a low-bandwidth radio-frequency excitation pulse to alternatingly shift the displaced excitation bands outside the imaging subject. Demonstration of this technique is presented using ^{1}H phantom and in vivo mouse renal hyperpolarized ^{13}C imaging experiments with conventional chemical shift imaging and fast low-angle shot sequences.

Results—From phantom and *in vivo* mouse studies, the spectral selectivity of the proposed method is readily demonstrated using results of chemical shift spectroscopic imaging, which displayed clearly delineated images of different metabolites. Imaging results using the proposed method without spectral encoding also showed effective separation while also providing high spatial resolution.

Conclusion—This method provides a way to acquire spectrally selective hyperpolarized ^{13}C metabolic images in a simple implementation, and with potential ability to support combination with more elaborate readout methods for faster imaging.

Correspondence to: Dong-Hyun Kim, Ph. D, Department of Electrical and Electronic Engineering, Engineering Hall 3, Room C228, Yonsei University, Seoul, Korea 120-749, Tel: +82-2-2123-5874, Fax: +82-2-313-2879, donghyunkim@yonsei.ac.kr.

Presented in part at the 22th Annual Meeting of the ISMRM, Milan, Italy 2014

Keywords

hyperpolarized; ^{13}C; metabolic imaging; chemical shift displacement; 9.4T

Introduction

Spectroscopic imaging with hyperpolarized ^{13}C compounds has been widely used recently to acquire metabolism kinetics *in vivo*, where dynamic nuclear polarization (DNP) of ^{13}C and its rapid dissolution into aqueous state enables over 10,000-fold signal increase compared to conventional methods (1,2). Recent studies focused on imaging the signal arising from metabolic conversion processes of [1-^{13}C] pyruvate into lactate, alanine, bicarbonate, etc., thereby providing spatially varying metabolite images depending on tumor type (3,4), therapeutic responses (5, 6), and tissue viabilities (7–9). Also, some previous studies worked on detecting metabolic changes in the kidney, due to their importance and usefulness in early assessment of diseases such as diabetes (10,11) and acute tubular necrosis (12). Due to the limited lifetime of hyperpolarized signals, imaging strategies were primarily dedicated to accelerating the acquisition time using fast readouts such as echo planar imaging (13) and spiral (14,15), or by applying compressed sensing (16,17).

A number of studies involving hyperpolarized ^{13}C substrates were performed in ultra-high field (≥7T) environments by acquiring frequency-specific images with higher spatial resolution using frequency-selective steady-state free precession (SSFP) acquisition (18) or multi-band frequency encoding method (19). Frequency-selective methods are chosen partly due to the fact that common slice-selective acquisition methods are much more vulnerable to increased chemical shift displacement artifact along the slice direction, which results from wider spectral dispersion of resonances. To address this issue, several studies have been proposed for 3T settings where spectral-spatial pulses were used to overcome the spatial chemical shift displacement along the slice direction (20–22) while also increasing product SNR and preserving the magnetization of hyperpolarized substrate.

In this work, the displacement artifact arising from wide dispersion of chemical shifts at ultra-high field utilized in acquiring spectrally-selective hyperpolarized ^{13}C images. Instead of using multi-band frequency encoding methods, the slice-selection gradient reversal technique (23) is combined with low-bandwidth excitation RF pulse for acquiring signals from different metabolites in an interleaved manner at every TR. However, since translation of spin-echo based technique with 90°–180° RF pulses is difficult for hyperpolarized ^{13}C studies, the amount of spatial chemical shift caused by low-bandwidth RF excitation pulse is calculated to place the excitation band for different resonances outside the imaging body, thereby providing spectral and spatial selectivity simultaneously. This technique is demonstrated for acquiring coronal [1-^{13}C] pyruvate and lactate images in a single scan for mouse kidney *in vivo* at 9.4T.

Methods

MR Hardware and Pulse Sequence

Slice-selection with weak gradients causes the spectral dispersion between the excited metabolites to be extended outside the subject. Frequency-selective metabolic images can then be acquired in an interleaved manner by reversing the gradient polarity to excite the target slice and the slice outside the subject alternatively, similar to common slice-interleaved acquisition scheme (Fig 1a). To achieve this, the slice-selection gradients were modified from a conventional slice-selective chemical shift imaging (CSI) sequence and fast low-angle shot (FLASH) sequence as shown in Fig 1b. The required minimum shift distance can be determined from a ^{1}H scout image across the region of interest, as shown in Eq. [1]:

$$\Delta \mathrm{d} = \frac{\Delta f(\mathrm{Hz}) \cdot \mathrm{SliceThickness(mm)}}{RF_{BW}(\mathrm{Hz})} \quad [1]$$

where Δd and Δf represents spatial shift distance and spectral chemical shift, respectively, and bandwidth refers to the excitation RF bandwidth. Here, focused on renal imaging, selecting 5mm slices with 10mm shift distance, and chemical shift between [1-^{13}C] pyruvate and lactate of 1250Hz, the required RF bandwidth becomes 625Hz. Using a Gaussian excitation RF pulse (time-bandwidth product (TBW) = 2.7), the pulse width then becomes 4.4ms. All experiments were performed on a 9.4T Bruker BioSpec 94/20 USR small animal imaging system (Bruker BioSpin MRI GmbH, Ettlingen, Germany) equipped with ^{1}H-^{13}C dual-tuned mouse volume transmit/receive quadrature coil (40mm inner diameter) and actively shielded gradients (strength: 440 mT/m, maximum linear slew rate: 3440 T/m/s).

Numerical Simulations

To enable spectral selectivity by utilizing the chemical shift displacement ‘artifact’, residual excitation from neighboring resonances must be accounted for. Simulations were conducted to quantify the effect of sequence parameters related to the excitation RF pulse on spatial displacement distance and signal contamination level. The amount of signal contamination were calculated at a given imaging slice thickness and spatial displacement distance for spectral dispersion of lactate from pyruvate-hydrate (~400Hz) and pyruvate (~1250Hz) at 9.4T. Slice thickness used during the simulation was fixed to 5mm to illustrate actual *in vivo* situation, and imaging slice depth with respect to subject’s extremity (5mm and 10mm) was varied. Here, the TBW of the simulated RF pulse profile was fixed to 2.7 to match the Gaussian RF pulse used during the *in vivo* experiments. Then, the excitation RF bandwidth was controlled by varying the RF pulse durations. Assuming homogenous spatial distribution of respective resonances, signal contamination was calculated by performing numerical integration of the area below the excitation RF profile which remained ‘inside’ the subject after inducing spatial displacement (red hash-marked area in Fig. 1d). The resulting values were normalized with respect to the highest contamination value obtained during the simulation.

Phantom Experiment

To validate the spectral selectivity of the proposed method, two cylindrical tubes (d = 1.6cm) filled with distilled water and acetone (98.0% purity) were tested. At 9.4T the chemical shift between water and acetone is 750Hz (data not shown). By selecting 6mm slice thickness and 12mm separation distance between slices, the required RF bandwidth then becomes 375Hz and the RF duration becomes 7.2ms. Reference coronal image of the phantoms were acquired with 2D multi-slice FLASH sequence, and spectrally-selective images were acquired with the proposed method implemented into a different version of FLASH sequence. Scan parameters were as follows: TR/TE = 120/16.3ms, 6mm slices, 12mm gap between slices (for spectrally-selective images), 30° flip angle, 40 × 40mm^2 FoV, and 256 × 256 matrix.

Sample Preparation and *in vivo* Experiments

[1-^{13}C] pyruvic acid (Cambridge Isotope, Tewksbury, MA) doped with 15mM Trityl radical OX-063 (Oxford instruments, Oxford, UK) and 1.5mM Dotarem (Guerbet, France) was polarized via dynamic nuclear polarization technique using HyperSense polarizer (Oxford Instruments, Oxford, UK). 3.8mL of Tris/EDTA (40mM Tris, 80mM NaOH, 2.0g/L EDTA, 50mM NaCl) solution was used for dissolution. Healthy balb/c nude mice received approximately 300ul of the hyperpolarized pyruvate substrate dosage with a pH of 7.4 through a tail vein catheter over a duration of 5s. Anesthesia was maintained using isoflurane at 1.5–3% and respiration was monitored throughout the experiments. Temperature was regulated by ventilated scanner bed with warm water at 37°C. All animal procedures were approved by the local animal care and use committee. For anatomical localization, T_2-weighted turbo-RARE ^{1}H MR images in the axial plane through the mouse kidney were acquired with an in-plane resolution of 0.156mm and 5mm slice thickness. Additional coronal slices were also acquired for the prescription of ^{13}C CSI and for overlaying the metabolic images. Before switching to ^{13}C acquisition mode an automatic, iterative global 1st and 2nd-order shimming was performed with the kidney placed at the center of the coil. ^{13}C transmit gain was calibrated prior to each animal experiment using an 8M [1-^{13}C] urea syringe phantom placed near the target anatomy.

For the mouse *in vivo* ^{13}C CSI experiment, the FoV was set to 80 × 40mm^2 for coronal coverage of the mouse body, with matrix size = 16 × 8 (5mm in-plane resolution), 5mm slice thickness, 10mm separation between slices, TR = 100ms (between excitation of same metabolite), spectral width = 6510 Hz, 512 spectral points, flip angle = 10°/ 5° for lactate / pyruvate were used. Total scan time for CSI acquisition was ~12s. Metabolite maps (interpolated, 128×256) were generated from ~50Hz from lactate and pyruvate peaks. Similar modifications were made for FLASH sequence to obtain images without spectral encoding. This allowed interleaved acquisition of two different metabolite signals at every TR, with centric phase encoding order implemented to enable fast acquisition of k-space center. Imaging parameters for FLASH were FoV = 40 × 40mm^2, matrix size = 32 × 32 (1.25mm in-plane resolution), 5mm slice thickness, 10mm separation between slices, TR / TE = 100 / 3.8ms, spectral width = 50000 Hz, flip angle = 20° / 5° for lactate / pyruvate, NEX = 4 (alternating between k-space lines of lactate and pyruvate, moving to next phase encoding line after NEX is done), resulting in total scan time of 12.8s. For both CSI and

FLASH experiments, signal acquisition started 15 seconds after the start of pyruvate injection, and the transmit/receive frequencies were adjusted according to the alternating gradient polarity at every TR.

Results

Simulation results of signal contamination level according to varying pulse sequence parameters are shown in Fig. 1d, along with illustration of change in the signal contamination area with respect to the excitation RF duration change (Fig. 1c). In Fig. 1d, solid and dotted lines represent different imaging slice depths of 5mm and 10mm, respectively (i.e. minimum spatial displacement distance). Contamination level is higher for pyruvate-hydrate than pyruvate due to smaller Δf. As the pulse duration increases (i.e. as bandwidth decreases under fixed TBW), the displacement distance becomes farther and the signal contamination from neighboring resonances decreases.

Selective images of water and acetone phantoms shown in Fig. 2 display effective spectral suppression of other spins. In the reference image (Fig. 2a), the measured peak signal level of acetone was approximately 50% of the water signal, as shown in the line plot (bottom row). Comparing the spectrally-selective images, the measured residual signal levels of acetone and water were less than 1% in respective images shown in Fig. 2b and Fig. 2c.

Figure 3a shows the full coverage of mouse body with CSI voxel positions overlaid as reference. Results of the CSI acquisition using the proposed method are presented in Fig. 3b–c. Signals from lactate and pyruvate can be observed, where high LDH activity in two renal cortices results in high lactate signal (Fig 3b), while venous perfusion of injected pyruvate results in dominant pyruvate signal from the vena cava. Representative magnitude spectra obtained with the CSI acquisition at voxels located at both kidneys and the vein region can be seen in Figs. 3b–c (2^{nd} and 3^{rd} columns). Pyruvate and lactate signals are effectively suppressed in respective images, demonstrating the spectral selectivity of the proposed method. Small residual signal from pyruvate-hydrate can be observed in the lactate spectra, with measured signal level less than 10% of lactate peak signal.

With the proposed method implemented in FLASH sequence, metabolic images of lactate and pyruvate were also acquired. The results are shown in Fig. 4, along with ^{1}H anatomical reference image covering the same coronal FoV (Fig. 4a). The slice centered at the kidneys was used here, with each ^{13}C image averaged 4 times to increase the SNR. As expected, major source of lactate signal was from the renal region, especially toward the center area where renal artery meets the renal pelvis. Again, highest pyruvate signal was observed inside the vena cava due to perfusion of the injected substrate.

Discussions and Conclusion

A simple method was proposed for the spectrally-selective acquisition of *in vivo* hyperpolarized ^{13}C images in ultrahigh field strength. Large spatial chemical shift displacement was induced by low-bandwidth excitation RF pulse, while signals from different metabolites were acquired in an interleaved fashion. This method is demonstrated by imaging *in vivo* ^{13}C lactate and pyruvate, using CSI and 2D multi-slice FLASH

sequences. Since the excitation band is moved outside the body during acquisition of different resonances to achieve spectral selectivity, the proposed method can remove complications arising from applying spatial-, spectral- or spectral-spatial excitations of different body regions where perfusion into the area of interest may occur. The proposed method can also be combined with fast readout methods to achieve higher temporal or in-plane resolution. At its current form, the proposed method requires relatively large number of excitations due to its Cartesian readout scheme. However, by implementing spiral or EPI readouts, the amount of excitations can be significantly reduced and thus help effective usage of the hyperpolarized magnetization of the injected substrate, and potentially increase the SNR of individual time points to a sufficient level at which time-resolved acquisition can be performed to measure the metabolite kinetics. The SNR provided by time-resolved acquisition using the proposed method, with the current implementation, was insufficient, thus single time-point imaging with multiple averages were chosen.

Imaging results shown in Fig. 4 demonstrates clearly delineated signals from lactate and pyruvate without major contamination effects. For contamination effects from residual excitation of neighboring pyruvate-hydrate to be seen in the lactate-only image (Fig. 4b), the spatial distribution of highest lactate signal should follow the pyruvate signal distribution, as pyruvate-hydrate is observed primarily along with pyruvate. The fact that the medial ends of both kidneys display lower signal intensity supports that the contamination effects are minimal. However, contamination resulting from insufficient spatial displacement or broad slice profile could be a major limiting factor in quantitative applications. As shown in Fig. 1d, using longer RF pulses will enhance the spectral selectivity at the expense of SNR loss due to T2* effects. As expected, as imaging slice depth increases, the amount of signal contamination also increases. This is due to the fact that the displacement distance must also be set farther to push the unwanted excitation band outside the subject body. To effectively suppress the pyruvate-hydrate signal (~400Hz from lactate) in cases where the imaging slice depth is e.g. 10mm, the RF duration needs to be up to ~15ms under the implemented excitation RF pulse with TBW of 2.7. In terms of imaging slice position, the displacement distance must be set far compared to the distance used in this study for the proposed method to work at the abdomen level. Since the RF bandwidth will need to be lower, this will cause the slice-selection gradient duration to be longer, diminishing the SNR due to T2*. Also, separation of resonances which are spectrally located closer to one another will face similar limitation from T2*. For example, resolving alanine and pyruvate-hydrate in two different slices would require significantly lower bandwidth due to their spectral proximity (~250Hz at 9.4T). Using an excitation RF pulse with lower TBW can therefore be beneficial in these cases since the bandwidth will be lower at a given RF duration. However, since RF pulses with low TBW generally have relatively broad slice profile, the tradeoff between metabolite SNR and residual excitation should be considered. Similarly, extension of this method to axial slices face T2* limits as well since the displacement distance must be set even farther compared to the coronal case. To avoid this SNR loss, axial acquisition along with application of preparation modules such as spatial saturation at the position where the ‘shifted’ slice is located maybe considered. However, since saturation pulses will cause complete loss of acquired magnetization of the substrate, factors such as pulses’ spatial width and timing should be carefully calculated.

At 9.4T environment, *in vivo* T2* value for ^{13}C pyruvate ranges between 10 to 20ms (empirically measured at 9.4T under similar conditions, data not shown), possibly making direct application difficult for common spectral-spatial excitation RF pulses with lengths at the range of 15 to 20ms (20–22). With much faster *in vivo* T2* decay, SNR of hyperpolarized compounds can be compromised by the long RF duration of spectral-spatial pulses, along with increased sensitivity to motion and field inhomogeneity effects (25). Typically, higher field strength requires the subpulse durations to be shorter than those used in lower fields when the desired RF profile needs to be maintained. This will increase the minimum slice thickness and impose further design constraints (25). Furthermore, any gradient performance-related issues such as gradient delay and eddy currents can cause unwanted excitation / suppression of neighboring resonances in the spectra (26).

With the current implementation of the proposed method, the number of different chemical species that are simultaneously acquired is limited to two. Potential applications can therefore be studies involving the observation of two particular metabolites, including the now-standard [1-^{13}C] pyruvate conversion to ^{13}C lactate via lactate dehydrogenase (LDH) enzyme activity. Another potential application includes pH imaging using hyperpolarized ^{13}C bicarbonate to observe bicarbonate and CO_2, where the Henderson-Hasselbalch equation can be applied to calculate *in vivo* pH after the acquisition of individual signals (27). Other applications may include assessment tumor grade for subcutaneous animal models, along with acquisition of 13C images for *in vivo* muscle metabolism. Both of these applications are facilitated by the fact that the region of interest is located near the extremity of the body, thus less constrained by the required minimum spatial displacement along the chosen slice-selection direction. For separating more than two species, changes to the slice-selection gradient amplitude needs to be introduced in addition to the polarity switching at every TR. Multiple displacement bands can be created based on the calculation of displacement distance given in Eq. [1]. However, since interleaved acquisition for multiple resonances will also increase total acquisition time, optimization of parameters such as displacement distance and RF bandwidth is required.

Acknowledgements

The authors would like to thank Eunkyung Wang for her animal handling efforts. This work was financially supported by the Korean Health Technology R&D Project, Ministry for Health, Welfare & Family Affairs.

References

1. Ardenkjaer-Larsen JH, Fridlund B, Gram A, Hansson G, Hansson L, Lerche MH, Servin R, Thaning M, Golman K. Increase in signal-to-noise ratio of > 10,000 times in liquid-state NMR. Proc Natl Acad Sci USA. 2003; 100:10158–10163. [PubMed: 12930897]
2. Golman K, Ardenkjaer-Larsen JH, Petersson JS, Mansson S, Leunbach I. Molecular imaging with endogenous substances. Proc Natl Acad Sci USA. 2003; 100:10435–10439. [PubMed: 12930896]
3. Golman K, Zandt RI, Lerche M, Pehrson R, Ardenkjaer-Larsen JH. Metabolic imaging by hyperpolarized ^{13}C magnetic resonance imaging for in vivo tumor diagnosis. Cancer Res. 2006; 66:10855–10860. [PubMed: 17108122]
4. Chen AP, Albers MJ, Cunningham CH, Kohler SJ, Yen YF, Hurd R, Tropp J, Bok R, Pauly JM, Nelson SJ, Kurhanewicz J, Vigneron DB. Hyperpolarized C-13 spectroscopic imaging of the TRAMP mouse at 3T-initial experience. Magn Reson Med. 2007; 58(6):1099–1106. [PubMed: 17969006]

5. Day SE, Kettunen MI, Gallagher FA, Hu DE, Lerche M, Wolber J, Golman K, Ardenkjaer-Larsen JH, Brindle KM. Detecting tumor response to treatment using hyperpolarized ^{13}C magnetic resonance imaging and spectroscopy. Nat Med. 2007; 13(11):1382–1387. [PubMed: 17965722]
6. Park JM, Recht LD, Josan S, Merchant M, Jang T, Yen YF, Hurd RE, Spielman DM, Mayer D. Metabolic response of glioma to dichloroacetate measured in vivo by hyperpolarized ^{13}C magnetic resonance spectroscopic imaging. Neuro Oncol. 2013; 15(4):433–441. [PubMed: 23328814]
7. Hu S, Chen AP, Zierhut ML, Bok R, Yen YF, Schroeder MA, Hurd R, Nelson SJ, Kurhanewicz J, Vigneron DB. In vivo carbon-13 dynamic MRS and MRSI of normal and fasted rat liver with hyperpolarized ^{13}C-pyruvate. Mol Imaging Biol. 2009; 11(6):399–407. [PubMed: 19424761]
8. Golman K, Petersson JS, Magnusson P, Johansson E, Akeson P, Chai CM, Hansson G, Masson S. Cardiac metabolism measured noninvasively by hyperpolarized ^{13}C MRI. Magn Reson Med. 2008; 59(5):1005–1013. [PubMed: 18429038]
9. Schroeder MA, Lau AZ, Chen AP, Gu Y, Nagendran J, Barry J, Hu X, Dyck JR, Tyler DJ, Clarke K, Connelly KA, Wright GA, Cunningham CH. Hyperpolarized ^{13}C magnetic resonance reveals early- and late-onset changes to in vivo pyruvate metabolism in the failing heart. Eur J Heart Fail. 2013; 15(2):130–140. [PubMed: 23258802]
10. Laustsen C, Østergaard JA, Lauritzen MH, Nørregaard R, Bowen S, Søgaard LV, Flyvbjerg A, Pedersen M, Ardenkjaer-Larsen JH. Assessment of early diabetic renal changes with hyperpolarized [1-13C] pyruvate. Diabetes Metab Res Rev. 2013; 29(2):125–129. [PubMed: 23166087]
11. Keshari KR, Wilson DM, Sai V, Bok R, Jen KY, Larson P, Van Criekinge M, Kurhanewicz J, Wang ZJ. Noninvasive in vivo imaging of diabetes-induced renal oxidative stress and response to therapy using hyperpolarized 13C dehydroascorbate magnetic resonance. Diabetes. 2015; 64(2): 344–352. [PubMed: 25187363]
12. Clatworthy MR, Kettunen MI, Hu DE, Mathews RJ, Witney TH, Kennedy BWC, Bohndiek SE, Gallagher FA, Jarvis LB, Smith KGC, Brindle KM. Magnetic resonance imaging with hyperpolarized [1, 4-^{13}C2] fumarate allows detection of early renal acute tubular necrosis. PNAS. 2012; 109(33):13374–13379. [PubMed: 22837393]
13. Cunningham CH, Chen AP, Albers MJ, Kurhanewicz J, Hurd RE, Yen YF, Pauly JM, Nelson SJ, Vigneron DB. Double spin-echo sequence for rapid spectroscopic imaging of hyperpolarized ^{13}C. J Magn Reson. 2007; 187(2):357–362. [PubMed: 17562376]
14. Mayer D, Yen YF, Tropp J, Pfefferbaum A, Hurd RE, Spielman DM. Application of subsecond spiral chemical shift imaging to real-time multislice metabolic imaging of the rat in vivo after injection of hyperpolarized ^{13}C1- pyruvate. Magn Reson Med. 2009; 62(3):557–564. [PubMed: 19585607]
15. Josan S, Spielman DM, Yen YF, Hurd RE, Pfefferbaum A, Mayer D. Fast volumetric imaging of ethanol metabolism in rat liver with hyperpolarized [1-^{13}C]pyruvate. NMR Biomed. 2012; 25(8): 993–999. [PubMed: 22331837]
16. Hu S, Lustig M, Chen AP, Crane J, Kerr A, Kelley DA, Hurd RE, Kurhanewicz J, Nelson SJ, Pauly JM, Vigneron DB. Compressed sensing for resolution enhancement of hyperpolarized ^{13}C flyback 3D-MRSI. J Magn Reson. 2008; 192(2):258–264. [PubMed: 18367420]
17. Larson PE, Hu S, Lustig M, Kerr AB, Nelson SJ, Kurhanewicz J, Pauly JM, Vigneron DB. Fast dynamic 3D MR spectroscopic imaging with compressed sensing and multiband excitation pulses for hyperpolarized ^{13}C studies. Magn Reson Med. 2011; 65(3):610–619. [PubMed: 20939089]
18. von Morze C, Sukumar S, Reed GD, Larson PE, Bok RA, Kurhanewicz J, Vigneron DB. Frequency-specific SSFP for hyperpolarized ^{13}C metabolic imaging at 14.1T. MagnReson Imaging. 2013; 31(2):163–170.
19. Ramirez MS, Lee J, Walker CM, Sandulache VC, Hennel F, Lai SY, Bankson JA. Radial spectroscopic MRI of hyperpolarized [1-^{13}C] pyruvate at 7 tesla. Magn Reson Med. 2014; 72(4): 986–995. [PubMed: 24186845]
20. Larson PE, Kerr AB, Chen AP, Lustig MS, Zierhut ML, Hu S, Cunningham CH, Pauly JM, Kurhanewicz J, Vigneron DB. Multiband excitation pulses for hyperpolarized ^{13}C dynamic chemical-shift imaging. J Magn Reson. 2008; 194(1):121–127. [PubMed: 18619875]

21. Lau AZ, Chen AP, Ghugre NR, Ramanan V, Lam WW, Connelly KA, Wright GA, Cunningham CH. Rapid multislice imaging of hyperpolarized ^{13}C pyruvate and bicarbonate in the heart. Magn Reson Med. 2010; 64(5):1323–1331. [PubMed: 20574989]

22. Schulte RF, Sperl JI, Weidl E, Menzel MI, Janich MA, Khegai O, Durst M, Ardenkjaer-Larsen JH, Glaser SJ, Haase A, Schwaiger M, Wiesinger F. Saturation-recovery metabolic-exchange rate imaging with hyperpolarized [1-^{13}C] pyruvate using spectral-spatial excitation. Magn Reson Med. 2013; 69(5):1209–1216. [PubMed: 22648928]

23. Park HW, Kim DJ, Cho ZH. Gradient reversal technique and its applications to chemical-shift-related NMR imaging. Magn Reson Med. 1987; 4(6):526–536. [PubMed: 3613953]

24. Tang H, Wu EX, Kennan R, Liu H, Williams DS. Interleaved water and fat imaging and application to lipid quantitation using the gradient reversal technique. J Magn Reson. 2007; 26:1064–1070.

25. Zur Y. Design of improved spectral-spatial pulses for routine clinical use. Magn Reson Med. 2000; 43(3):410–420. [PubMed: 10725884]

26. Bernstein, MA.; King, KF.; Zhou, XJ. Handbook of MRI Pulse Sequences. Burlington: Elsevier Academic Press; 2004. Eddy-Current Compensation; p. 319-330.

27. Gallagher FA, Kettunen MI, Day SE, Hu DE, Ardenkjaer-Larsen JH, Zandt R, Jensen PR, Karlsson M, Golman K, Lerche MH, Brindle KM. Magnetic resonance imaging of pH in vivo using hyperpolarized 13C-labelled bicarbonate. Nature. 2008; 453(7197):940–943. [PubMed: 18509335]

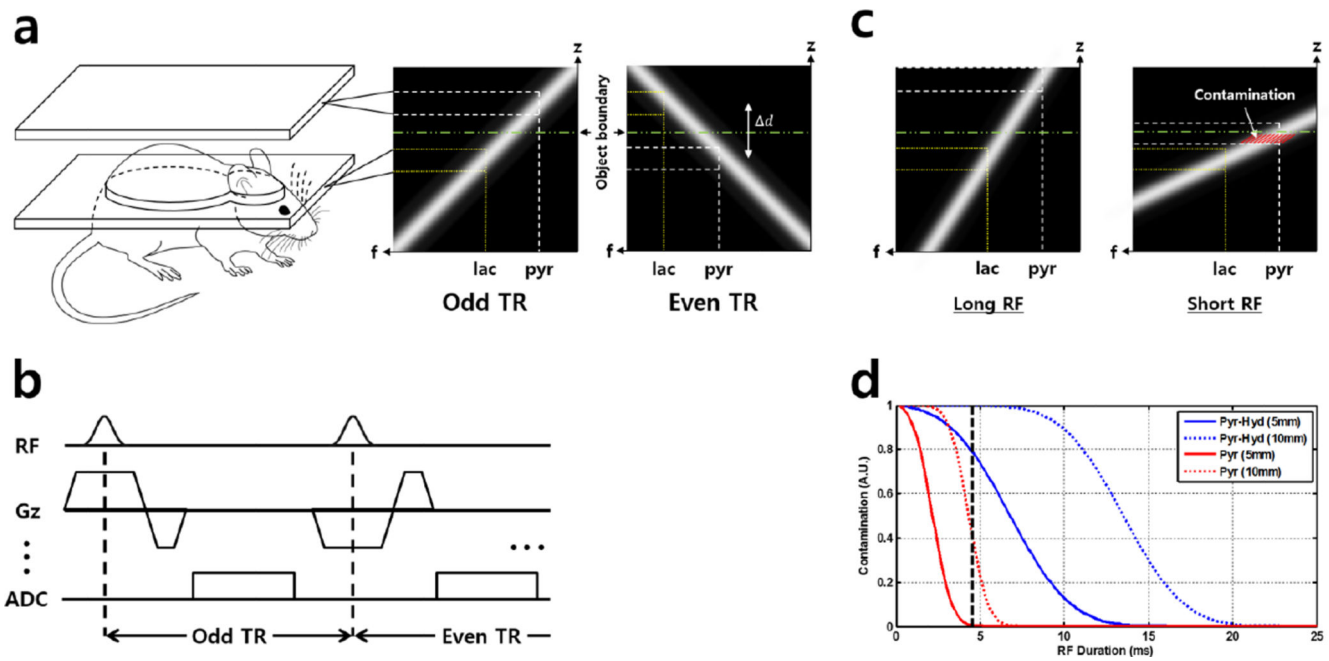

Figure 1.

Graphical illustration of the proposed acquisition method based on spatial chemical shift displacement. (a) Acquisition is done in a slice-interleaved manner, resolving two different resonances at two different slices. In the excitation profile of the proposed method (a, right), the spectral selectivity is achieved via chemical shift displacement along the slice (z)-direction, resolving lactate (dotted, yellow line) and pyruvate (dotted, white line) in two different slices. (b) Simplified pulse sequence diagram. (c) Under fixed imaging slice depth, displacement distance is controlled by varying excitation RF pulse duration. Contamination arises when slice profile of the displaced band overlaps with the subject body (red hash-marked area). Here, long and short RF refers to relative pulse durations. (d) Simulation results. Solid and dotted curves indicate different imaging slice depths (5 and 10mm, respectively), and red and blue colors indicate different metabolites (pyruvate and pyruvate-hydrate, respectively). Under fixed TBW, increasing RF durations decreases its bandwidth, thereby creating farther spatial displacement between neighboring resonances and facilitating the proposed spectrally-selective acquisition method. RF pulse length used in this study is marked by black dashed-line (4.5ms)

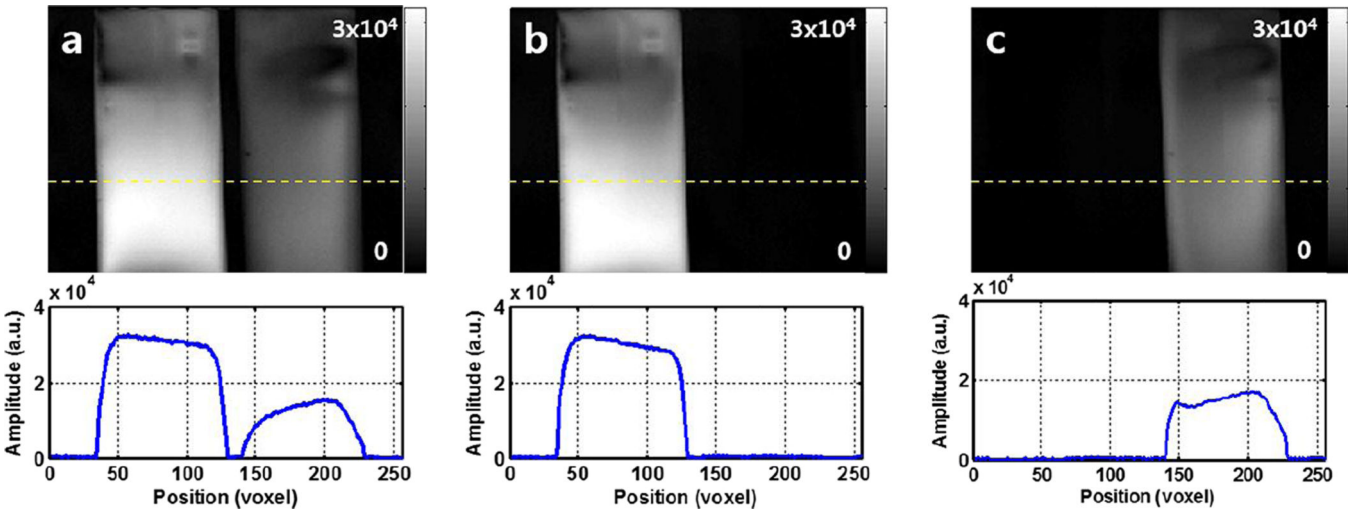

Figure 2.

Results of 1H phantom experiment. (a) Reference image showing both water (left) and acetone (right) phantoms in a single slice. (b) and (c) displays water- and acetone-only images, respectively, acquired simultaneously using the proposed method. Test tubes filled with water and acetone are completely separated in respective images via spatial chemical shift displacement along the slice direction, demonstrating the spectral selectivity of the proposed method.

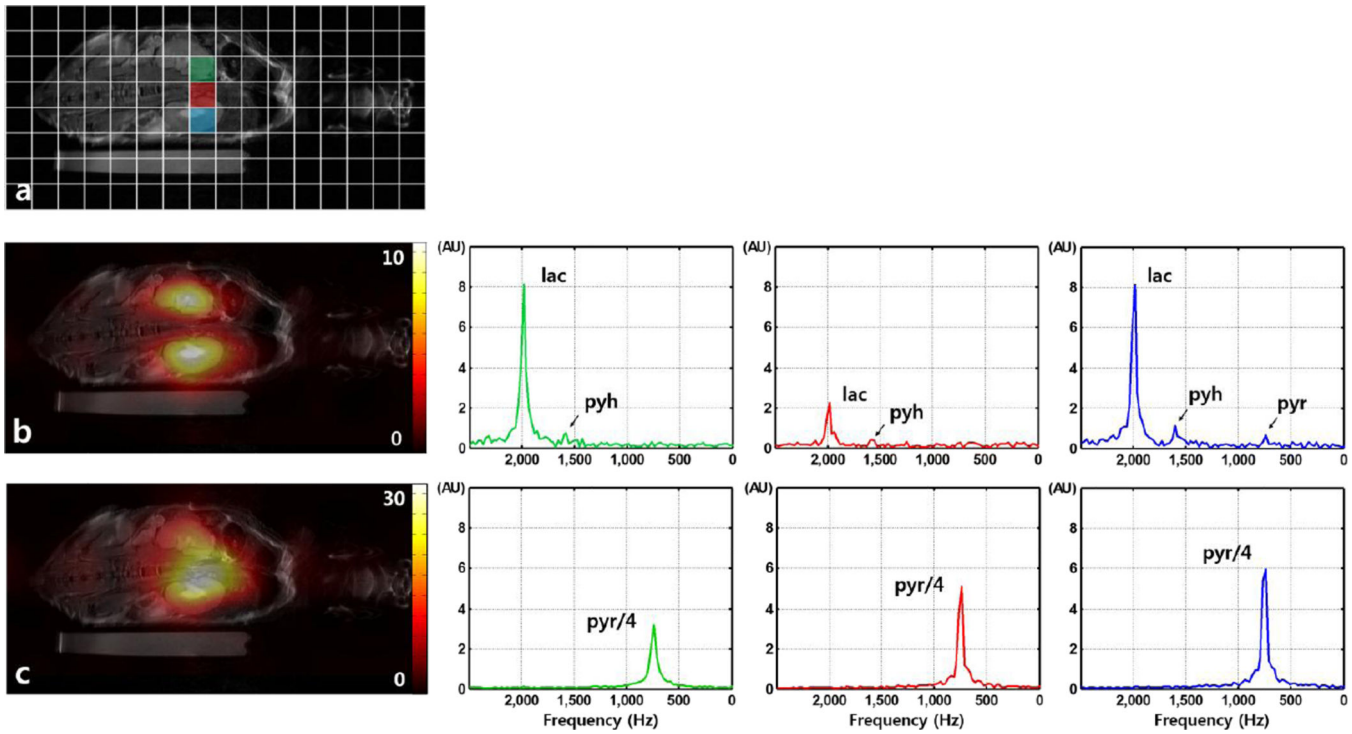

Figure 3.

Results of slice-selective CSI acquisition with the proposed method. (a) Reference coronal 1H anatomical image with CSI voxel position overlay. Representative voxels are marked in colors green, red and blue. (b) Acquired lactate image (‘image 1’) overlaid on 1H proton image, and individual spectra from the representative voxels. High LDH activity in the renal cortex results in subsequent high lactate signal. (c) Acquired pyruvate image (‘image 2’), and individual spectra from the representative voxels. High perfusion of injected pyruvate can be observed inside the vena cava. Spectra from lactate and pyruvate images were plotted separately using same scales for comparison, and pyruvate signal was scaled to fit the set amplitude range.

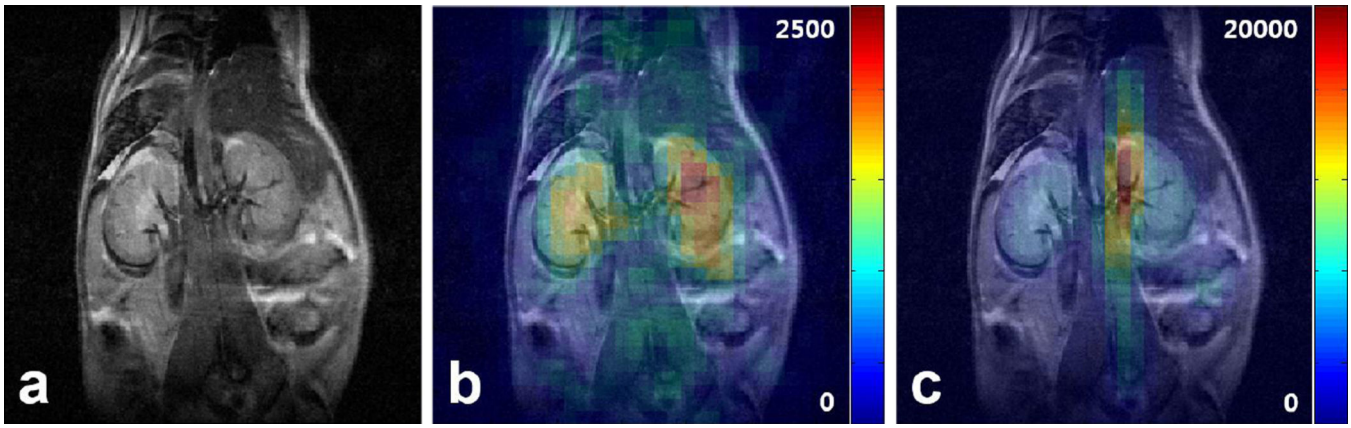

Figure 4.

Results of slice-selective FLASH acquisition with the proposed method. (a) Reference coronal 1H anatomical image over the renal region. Acquired (b) lactate and (c) pyruvate images. Lactate and pyruvate signals are localized to renal and venal areas, respectively as expected from the CSI results. The PSF provided by FLASH sequence allows enhanced spatial resolution for observation of both metabolites.